Journal of Sound and Vibration (1998) **215**(5), 997–1014
Article No. sv981579

VIBRATION TRANSMISSION THROUGH SELF-ALIGNING (SPHERICAL) ROLLING ELEMENT BEARINGS: THEORY AND EXPERIMENT

T. J. Royston and I. Basdogan†
Vibrations and Acoustics Laboratory, *Department of Mechanical Engineering*,
The University of Illinois at Chicago, *Chicago*, *IL* 60607-7022, *U.S.A.*

(*Received* 25 *July* 1997, *and in final form* 20 *February* 1998)

Interest in vibration control in systems employing rolling element bearings, ranging from rotor systems used in energy conversion/transmission to high-precision, multi-degree-of-freedom optical positioning systems, has focused attention on the modelling of bearing dynamic stiffness properties. While modelling a rolling element bearing either as an ideal boundary condition for a shaft or as a simple translational element may suffice in understanding basic rotor system dynamics, such simple models are inadequate in explaining how vibratory energy may be transmitted from, for example, transverse shaft vibrations to perpendicular, out-of-plane casing vibrations. Recently, researchers have begun to address this issue for conventional single row ball or cylindrical rolling element bearings which exhibit a strong moment–coupling stiffness. The study reported in this article focuses on double row spherical (self-aligning) rolling element bearings where moment stiffnesses are negligible, but translational cross-coupling stiffnesses between axial and radial bearing directions are present. A new theoretical model for the direct and cross-coupling stiffness coefficients of spherical rolling element bearings is developed and partially validated using new experimental techniques. It is shown that the coefficient values are complicated functions dependent on radial and axial preloads. While cross-coupling stiffness coefficients are negligible with simple radial *or* axial preloads, under the combined radial *plus* axial preload condition, the cross-coupling stiffness coefficient between the axial direction and the direction of the radial preload becomes significant.

1. INTRODUCTION

Interest in vibration control in systems employing rolling element bearings, ranging from rotor systems used in energy conversion/transmission [1, 2] to high-precision, multi-degree-of-freedom optical positioning systems [3], has focused attention on the modelling of bearing dynamic stiffness properties. While modelling a rolling element bearing either as an ideal boundary condition for a shaft or as a simple translational stiffness element may suffice in understanding basic rotor system dynamics, such simple models are inadequate in explaining how vibratory energy may be transmitted from, for example, transverse shaft vibrations to perpendicular, out-of-plane casing vibrations. A vibration model of a system similar to Figure 1, based on simple direct translational stiffness bearing models, can predict only purely in-plane type motion on the flexible casing plate given only the bending motion of the shaft. However, the dominant casing plate motion is typically flexural or out-of-plane.

† Present address: Jet Propulsion Laboratory, Pasadena, CA 91109, U.S.A.

0022–460X/98/350997 + 18 $30.00/0

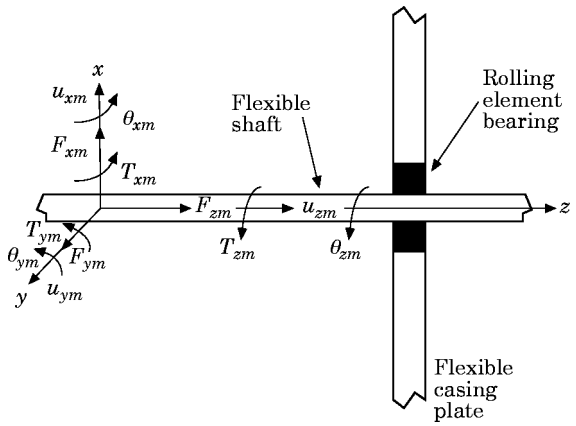

Figure 1. Schematic representation of the vibration transmission problem. Here the flexible shaft is subjected to mean forces F_{im} and torques T_{im}, where $i = x, y, z$ is the direction and subscript m implies mean. Also, θ is the angular displacement and **u** is the translational displacement.

In a recent series of articles by Lim and Singh [4–6], this issue was addressed for conventional single row ball or cylindrical rolling element bearings which exhibit a strong moment stiffness which couples the transverse shaft vibrations to the transverse casing plate vibrations of Figure 1. The study reported in this article compliments the studies of Lim and Singh by considering double-row spherical (self-aligning) rolling element bearings where moment stiffnesses are negligible, but translational cross-coupling stiffnesses between axial and radial bearing directions are present and may act as the dominant mechanism for the transmission of vibratory energy. In this article, a new theoretical formulation for the multi-dimensional, preload-dependent, spherical bearing stiffness matrix is offered and new experimental techniques to measure both direct and cross-coupling stiffness coefficients are presented and used to verify the theoretical formulation.

2. LITERATURE REVIEW

While a wide range of theoretical models of varying complexity can be found for conventional moment-carrying bearing stiffness properties, few studies exist specifically for spherical bearings. A study by Kleckner [7] focuses on the tribological issues of spherical bearing dynamic properties and actually uses the formulation of Harris [8] for calculation of the load-dependent direct translational stiffness values. To the authors' knowledge, only a handful of studies on any type of rolling element bearing have noted the existence of cross-coupling stiffness coefficients yielding a fully-populated multi-dimensional bearing stiffness matrix with each coefficient dependent on each term of the multi-dimensional static preloading condition. While Jones [9] did not actually define a bearing stiffness matrix, his theoretical formulations for ball and cylindrical rolling element bearing deformations under static loading conditions can be used to obtain fully populated stiffness matrices for conventional moment-carrying and single row spherical raceway bearings. Lim and Singh's [4] fully-populated stiffness matrix formulations for conventional moment-carrying bearings have been successfully used to model the vibratory behavior of flexible shaft–bearing–plate assemblies [5]. In these studies, it was found that moment stiffnesses and cross-coupling stiffness terms play a crucial role in vibration transmission.

No comparable studies can be found for self-aligning (spherical) bearings where the moment stiffnesses are negligible but cross-coupling stiffness coefficients may be significant.

Most experimental studies found in the literature [e.g. 10, 11] for obtaining stiffness values focus on the simple single-degree-of-freedom situation, considering radial or axial bearing vibrations/stiffness coefficients independently. Some studies also have considered large deformation across the bearing and consequently, non-linearities associated with the direct translational bearing stiffnesses [12].

3. ASSUMPTIONS AND OBJECTIVES

Conventional moment-carrying rolling element bearings can typically be placed into one of two groups, ball- or roller-type. Ball bearings have point contact under the no-load condition and elliptical contact under the loaded condition between the inner race, rolling element and outer race. Roller-types are cylindrical or conical, with a portion of straight contour on their contact dimension, with line contact under the no-load condition and rectangular contact under the loaded condition. While the contact angle α of ball bearings will change under load, α essentially remains unchanged under load for roller-type bearings. For these reasons, separate formulations for the stiffness of conventional ball and roller-type bearings are needed [4]. Spherical ball and roller type bearings, however, usually can be treated similarly. The spherical roller-type bearing has a fully crowned contour on its contact dimension. The radius of curvature of this contour will typically approach that of the inner and outer raceway curvature radii but not reach them [8]. Hence, theoretically both ball- and roller-type spherical bearings start with point/elliptical contact areas (except under heavy loading) and the contact angle α is a function of the load condition.

The mean bearing translational displacements $\mathbf{q}_m$ which are accompanied by mean load values $\mathbf{F}_m$ as shown in Figure 2 are given by the relative rigid body motions between the inner and outer rings. Note that angular displacements about the x and y axes need not be considered here since, due to the self-aligning nature of the spherical bearing, they are not opposed by moment loads. The total bearing displacement vector is given as $\mathbf{q} = \mathbf{q}_m + \mathbf{q}_a(t)$, where $\mathbf{q}_a(t)$ is the fluctuation about the mean point $\mathbf{q}_m$. In general, for small preloads and/or relatively large time dependent values of $\mathbf{q}_a(t)$, the bearing stiffness is time dependent and non-linear. In this study, the case where $\mathbf{q}_a(t)$ is very small relative to $\mathbf{q}_m$ is considered for which liearized bearing stiffness values can be employed. The basic

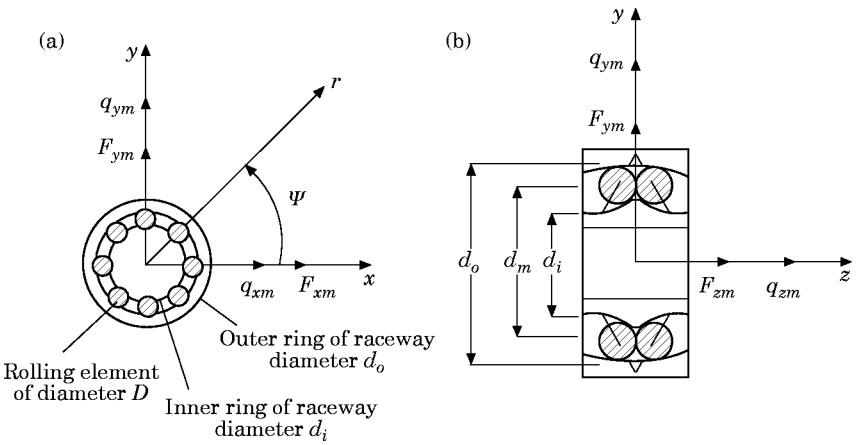

Figure 2. Spherical bearing kinematics and coordinate system: (a) front view, (b) enlarged side view.

load–deflection relation for each elastic rolling element is defined by the Hertzian contact stress theory [8], and the load experienced by each rolling element is described by its relative location in the bearing raceway. Further, in this study it is assumed that the angular position of each rolling element relative to one another is always maintained due to rigid cages. Secondary effects such as centrifugal forces and gyroscopic moments on the bearing due to extremely high rotational speeds are ignored. (Spherical bearings typically cannot be used in extremely high rotational speed applications, anyway [7].) Finally, tribological issues are beyond the scope of this study and hence in the present analysis the bearings are assumed to be unlubricated.

The specific objectives of this study are as follows: (1) to develop a new bearing stiffness matrix which is suitable for the analysis of vibration transmission through either ball or roller-type spherical bearings; (2) to develop an experimental technique to measure spherical bearing direct and cross-coupling stiffness coefficients as a function of axial and radial mean loads (preloads); (3) to verify the proposed stiffness model by comparing its predictions with experimental measurements; and (4) to relate the stiffness matrix values to various kinematic and design parameters, specifically unloaded contact angle and radial clearance, through parametric studies using the bearing stiffness matrix model.

4. THEORY

Consider the self-aligning double-row rolling element bearing shown in Figure 2. The relationships between the mean forces $\mathbf{F}_m = \{F_{xm}, F_{ym}, F_{zm}\}^T$ transmitted through the bearing and the resulting mean bearing displacements $\mathbf{q}_m = \{q_{xm}, q_{ym}, q_{zm}\}^T$ will be derived. From the bearing displacements the resultant elastic deformation $\delta(\Psi_j^i)$ of the jth rolling

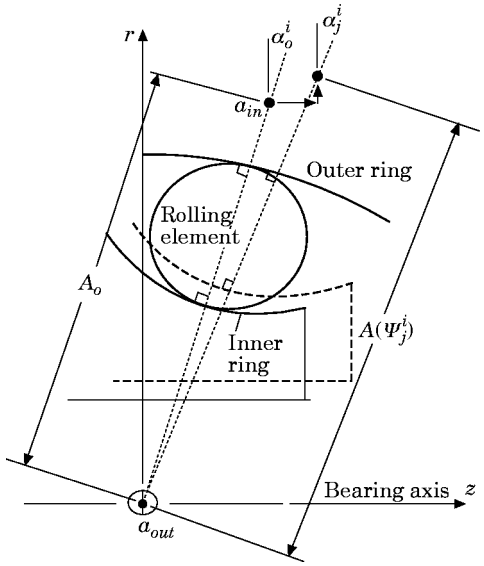

Figure 3. Elastic deformation of rolling element for non-constant contact angle α_j^i.

element of the ith row located at angle Ψ_j^i from the x-axis can be determined. Assuming the outer ring is fixed, in Figure 3 one has:

$$\delta(\Psi_j^i) = \begin{Bmatrix} A(\Psi_j^i) - A_0 & A(\Psi_j^i) > A_0 \\ 0 & A(\Psi_j^i) \leqslant A_0 \end{Bmatrix}, \qquad A(\Psi_j^i) = \sqrt{(\delta_{zj}^i)^2 + (\delta_{rj}^i)^2}\,,$$

$$\delta_{zj}^i = A_0 \sin(\alpha_0^i) + q_{zm} - P_e, \qquad \delta_{rj}^i = A_0 \cos(\alpha_0^i) + q_{xm} \cos(\Psi_j^i) + q_{ym} \sin(\Psi_j^i) - r_L. \tag{1a–d}$$

Here, A_0 and A are the unloaded and loaded relative distances between the inner (a_{in}) and outer (a_{out}) raceway groove curvature centers. Note that $A_0 = r_i$, the radius of the locus of inner raceway groove curvature centers. The unloaded contact angle is denoted by α_0^i and radial clearance and axial endplay are denoted by r_L and P_e, respectively. Axial endplay for a spherical bearing is related to radial clearance, r_L, as follows [8]:

$$P_e = 4r_0(\sin(\beta^i) - \sin(\alpha_0^i)) + 4r_L \sin(\alpha_0^i), \qquad \beta = \cos^{-1}\{(1 - r_L/r_0)\cos(\alpha_0^i)\}. \tag{2a–b}$$

Equations (1, 2) in conjunction with the Hertzian contact stress principle stated as follows yield the load deflection relationships for a single rolling element:

$$Q_j^i = K_n(\delta(\Psi_j^i))^n. \tag{3}$$

Here Q_j^i is the resultant normal load on the rolling element and K_n is the effective stiffness constant for the inner race–rolling element–outer race contacts and is a function of the bearing geometry and material properties. The exponent n will range from 3/2 to 10/9 depending on type of contact, going from point/elliptical to line/rectangular. The loaded contact angle α_j^i is given by

$$\tan(\alpha_j^i) = \delta_{zj}^i/\delta_{rj}^i. \tag{4}$$

The bearing stiffness matrix is a global representation of the bearing kinematic and elastic characteristics as it combines the effects of $2z$ number of loaded rolling element stiffnesses in parallel. Through vectoral sums $Q_j^i (i = 1, 2, j = x, y, z)$ in equation (3) for all of the loaded rolling elements one can relate the resultant bearing mean load vector $\mathbf{F_m}$ to the displacement vector $\mathbf{q_m}$:

$$\begin{Bmatrix} F_{xm} \\ F_{ym} \\ F_{zm} \end{Bmatrix} = \sum_{i=1}^{2} \sum_{j=1}^{z} Q_j^i \begin{Bmatrix} \cos(\alpha_j^i)\cos(\psi_j^i) \\ \cos(\alpha_j^i)\sin(\psi_j^i) \\ \sin(\alpha_j^i) \end{Bmatrix} = K_n \sum_{i=1}^{2} \sum_{j=1}^{z} \frac{\{\delta(\psi_j^i)\}^n}{A(\psi_j^i)} \begin{Bmatrix} \delta_{rj}^i \cos(\psi_j^i) \\ \delta_{rj}^i \sin(\psi_j^i) \\ \delta_{zj}^i \end{Bmatrix}. \tag{5}$$

Often, approximate integral forms of equation (5) are used instead of the summation forms to eliminate explicit dependence on Ψ_j^i. The summation form is retained here.

Now one defines a symmetric bearing stiffness matrix $\mathbf{K_{sb}}$ of dimension three from equation (5) and by assuming that $\mathbf{q_a} \ll \mathbf{q_m}$; i.e., the alternating component of the relative deflection across the bearing is much less than the mean component:

$$\mathbf{K_{sb}} = [\partial F_{pm}/\partial q_{sm}], \qquad p, s = x, y, z. \tag{6}$$

Here, each stiffness coefficient must be evaluated at the mean point $\mathbf{q_m}$. Note that $\mathbf{K_{sb}}$ is symmetric, i.e., $k_{ps} = k_{sp}$ and it may be fully populated:

$$\mathbf{K_{sb}} = \begin{bmatrix} k_{xx} & k_{xy} & k_{xz} \\ k_{yx} & k_{yy} & k_{yz} \\ k_{zx} & k_{zy} & k_{zz} \end{bmatrix}. \tag{7}$$

Using equation (7) the coefficients k_{ps} can be directly computed given the mean bearing displacement vector $\mathbf{q_m}$. However, usually it is the preload vector $\mathbf{F_m}$ which is known, not the resulting mean displacement vector. If this is the case, coupled non-linear equations (5) may be numerically solved beforehand to find $\mathbf{q_m}$ for a given $\mathbf{F_m}$. A very suitable approach is to use a Newton–Raphson methhod. This can be done by rearranging equation (5) as

$$\begin{Bmatrix} H_1 \\ H_2 \\ H_3 \end{Bmatrix} = \begin{Bmatrix} F_{xm} \\ F_{ym} \\ F_{zm} \end{Bmatrix} - \sum_{i=1}^{2} \sum_{j=1}^{z} Q_j^i \begin{Bmatrix} \cos(\alpha_j^i)\cos(\psi_j^i) \\ \cos(\alpha_j^i)\sin(\psi_j^i) \\ \sin(\alpha_j^i) \end{Bmatrix} = 0, \tag{8}$$

where $\mathbf{H} = \{H_1 \;\; H_2 \;\; H_3\}^{\mathrm{T}}$ are the determining functions to be minimized. By using Taylor's series, $\mathbf{H}$ may be expanded about a solution vector $\mathbf{q_m}$ by neglecting higher order terms:

$$\mathbf{H}(\mathbf{q_m} + \delta\mathbf{q_m}) \approx \mathbf{H}(\mathbf{q_m}) + \mathbf{J} \otimes \mathbf{q_m}, \tag{9}$$

where $\mathbf{J}$ is the Jacobian:

$$\mathbf{J} = \mathbf{K_{sb}} = [\partial F_{pm}/\partial q_{sm}], \qquad p, s = x, y, z. \tag{10}$$

The solution for $\mathbf{q_m}$ can be obtained by setting $\mathbf{H}(\mathbf{q_m} + \delta\mathbf{q_m}) = \mathbf{0}$ per equations (8–10) which yields a set of linear algebraic equations. The vector $\delta\mathbf{q_m}$ is added to the previously computed vector $\mathbf{q_m}$ for the next iteration until the convergence criterion, say $|\mathbf{H}(\mathbf{q_m})| < \varepsilon$ where ε is very small, is satisfied.

Note that the above formulation for the stiffness matrix is valid independently of angular misalignment about the x- and y-axis as defined in Figures 2 and 3 since the spherical bearing does not produce moment loads. The stiffness matrix is effectively defined with respect to a reference frame oriented with the unloaded inner raceway.

5. METHOD OF EXPERIMENTAL VALIDATION

In order to examine the validity of the theoretically developed bearing stiffness model, an experimental test has been devised. Consider using the bearing to connect two rigid bodies as denoted in Figure 4. Here, $\mathbf{r_1} = [r_{1x} \;\; r_{1y} \;\; r_{1z} \;\; \theta_{1x} \;\; \theta_{1y}]^{\mathrm{T}}$ and $\mathbf{r_2} = [r_{2x} \;\; r_{2y} \;\; r_{2z} \;\; \theta_{2x} \;\; \theta_{2y}]^{\mathrm{T}}$ denote the displacement of each rigid body form the static equilibrium position. Rotation about the z-axis for both rigid bodies is not considered as these axes are collocated with the bearing axial direction. The origin of the bearing co-ordinate system in both rigid body reference frames is given by $\mathbf{s_1} = [0 \;\; 0 \;\; L_1 \;\; 0 \;\; 0]^{\mathrm{T}}$ and $\mathbf{s_2} = [0 \;\; 0 \;\; -L_2 \;\; 0 \;\; 0]^{\mathrm{T}}$, respectively. Neglecting rotational motion of each rigid body about the z-axis, the entire system has 10 degrees of freedom. Five of these degrees represent system rigid body modes. Equations for the system are

$$\mathbf{M}\ddot{\mathbf{r}} + \mathbf{K}\mathbf{r} = \mathbf{F},$$

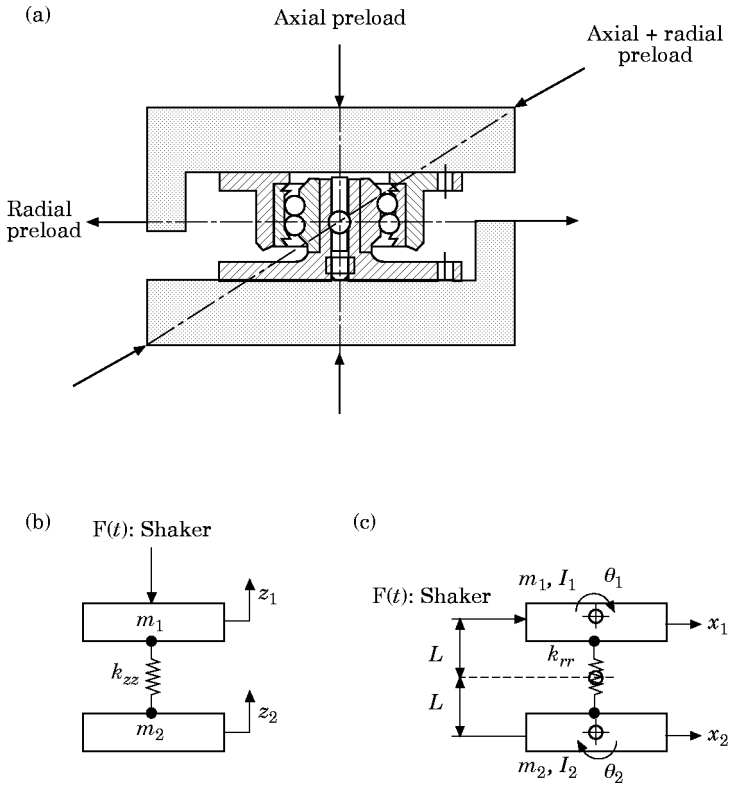

Figure 4. Experimental test set-up. (a) Self-aligning bearing with rigid masses of known inertia properties; (b) axial excitation; (c) radial excitation. Parameter values: $m_1 = 3{\cdot}366$ kg, $I_{1xx} = 0{\cdot}0114$ kg m^2, $I_{1yy} = 0{\cdot}0114$ kg m^2, $L_1 = 0{\cdot}0298$ m, $m_2 = 3{\cdot}133$ kg, $I_{2xx} = 0{\cdot}0113$ kg m^2, $I_{2yy} = 0{\cdot}0113$ kg m^2, $L_2 = 0{\cdot}0364$ m.

where

$$\mathbf{M} = \begin{bmatrix} \mathbf{M}_1 & 0 \\ \mathbf{0} & \mathbf{M}_2 \end{bmatrix}, \qquad \mathbf{M}_i = \begin{bmatrix} m_i & 0 & 0 & 0 & 0 \\ 0 & m_i & 0 & 0 & 0 \\ 0 & 0 & m_i & 0 & 0 \\ 0 & 0 & 0 & I_{ixx} & I_{ixy} \\ 0 & 0 & 0 & I_{iyx} & I_{iyy} \end{bmatrix}, \; i = 1, 2; \qquad \mathbf{r} = \begin{bmatrix} \mathbf{r}_1 \\ \mathbf{r}_2 \end{bmatrix},$$

$$\mathbf{K} = \begin{bmatrix} \mathbf{A}_1\mathbf{K}_{sb}\mathbf{A}_1^{\mathrm{T}} & \mathbf{A}_1\mathbf{K}_{sb}\mathbf{A}_2^{\mathrm{T}} \\ \mathbf{A}_2\mathbf{K}_{sb}\mathbf{A}_1^{\mathrm{T}} & \mathbf{A}_2\mathbf{K}_{sb}\mathbf{A}_2^{\mathrm{T}} \end{bmatrix},$$

$$\mathbf{A}_1 = \begin{bmatrix} -1 & 0 & 0 \\ 0 & -1 & 0 \\ 0 & 0 & -1 \\ 0 & L_1 & 0 \\ -L_1 & 0 & 0 \end{bmatrix}, \qquad \mathbf{A}_2 = \begin{bmatrix} 1 & 0 & 0 \\ 0 & 1 & 0 \\ 0 & 0 & 1 \\ 0 & L_2 & 0 \\ -L_2 & 0 & 0 \end{bmatrix}. \tag{11}$$

The external dynamic excitation force **F** may be applied to individual degrees of freedom or to combinations of degrees of freedom. Static preload forces are also applied in the axial

or radial x or y directions. Cases will be considered where the cross moments of inertia for the rigid bodies are zero, e.g.: $I_{ixy} = I_{iyx} = 0$, $i = 1, 2$.

First consider a preload applied only in the axial (z) or one of the radial (x or y) directions of the bearing. According to the developed theory, the off-diagonal terms of the stiffness matrix are zero. For harmonic excitation of frequency ω the following decoupled sets of equations are obtained:

$$\left\{ k_{xx} \begin{bmatrix} 1 & -L_1 & -1 & -L_2 \\ -L_1 & L_1^2 & L_1 & L_1L_2 \\ -1 & L_1 & 1 & L_2 \\ -L_2 & L_1L_2 & L_2 & L_2^2 \end{bmatrix} - \omega^2 \begin{bmatrix} m_1 & 0 & 0 & 0 \\ 0 & I_{1yy} & 0 & 0 \\ 0 & 0 & m_2 & 0 \\ 0 & 0 & 0 & I_{2yy} \end{bmatrix} \right\} \begin{bmatrix} r_{1x} \\ \theta_{1y} \\ r_{2x} \\ \theta_{2y} \end{bmatrix},$$

$$= \begin{bmatrix} F_{1x} \\ F_{\theta 1y} \\ F_{2x} \\ F_{\theta 2y} \end{bmatrix},$$

$$\left\{ k_{yy} \begin{bmatrix} 1 & L_1 & -1 & L_2 \\ L_1 & L_1^2 & -L_1 & L_1L_2 \\ -1 & -L_1 & 1 & -L_2 \\ L_2 & L_1L_2 & -L_2 & L_2^2 \end{bmatrix} - \omega^2 \begin{bmatrix} m_1 & 0 & 0 & 0 \\ 0 & I_{1xx} & 0 & 0 \\ 0 & 0 & m_2 & 0 \\ 0 & 0 & 0 & I_{2xx} \end{bmatrix} \right\} \begin{bmatrix} r_{1y} \\ \theta_{1x} \\ r_{2y} \\ \theta_{2x} \end{bmatrix},$$

$$= \begin{bmatrix} F_{1y} \\ F_{\theta 1x} \\ F_{2y} \\ F_{\theta 2x} \end{bmatrix},$$

$$\left\{ k_{zz} \begin{bmatrix} 1 & -1 \\ -1 & 1 \end{bmatrix} - \omega^2 \begin{bmatrix} m_1 & 0 \\ 0 & m_2 \end{bmatrix} \right\} \begin{bmatrix} r_{1z} \\ r_{2z} \end{bmatrix} = \begin{bmatrix} F_{1z} \\ F_{2z} \end{bmatrix}. \tag{12a–c}$$

Each set of coupled equations can be solved for its natural frequencies, all of which are zero (unconstrained rigid body motion) except for one in each case, regardless of stiffness coefficient values. The one non-zero natural frequency in each case, a, b, and c, is directly proportional to the corresponding stiffness coefficient, k_{xx}, k_{yy}, and k_{zz}, respectively. Hence, by appropriate excitation and measurement of system natural frequencies corresponding to the appropriate modes, values for the three diagonal terms of the bearing stiffness matrix, as a function of axial or radial preload, can be obtained experimentally.

Now consider a preload applied simultaneously in one of the radial (say x) and axial (z) directions. For this case, according to the developed theory, the stiffness coefficient

$k_{xz} = k_{zx}$ is the only non-zero off-diagonal term. Hence, equations (12a) and (12c) are replaced with a coupled set:

$$\left\{ \begin{bmatrix} k_{xx} \begin{bmatrix} 1 & -L_1 & -1 & -L_2 \\ -L_1 & L_1^2 & L_1 & L_1L_2 \\ -1 & L_1 & 1 & L_2 \\ -L_2 & L_1L_2 & L_2 & L_2^2 \end{bmatrix} & k_{xz} \begin{bmatrix} 1 & -1 \\ -L_1 & L_1 \\ -1 & 1 \\ -L_2 & L_2 \end{bmatrix} \\ k_{zx} \begin{bmatrix} 1 & -L_1 & -1 & -L_2 \\ -1 & L_1 & 1 & L_2 \end{bmatrix} & k_{zz} \begin{bmatrix} 1 & -1 \\ -1 & 1 \end{bmatrix} \end{bmatrix} \right.$$

$$\left. -\omega^2 \begin{bmatrix} m_1 & 0 & 0 & 0 & & \\ 0 & I_{1yy} & 0 & 0 & & \mathbf{0} \\ 0 & 0 & m_2 & 0 & & \\ 0 & 0 & 0 & I_{2yy} & & \\ & & & & m_1 & 0 \\ & \mathbf{0} & & & 0 & m_2 \end{bmatrix} \right\} \begin{bmatrix} r_{1x} \\ \theta_{1y} \\ r_{2x} \\ \theta_{2y} \\ r_{1z} \\ r_{2z} \end{bmatrix} = \begin{bmatrix} F_{1x} \\ F_{\theta 1y} \\ F_{2x} \\ F_{\theta 2y} \\ F_{1z} \\ F_{2z} \end{bmatrix}. \quad (13)$$

This system of equations has four zero natural frequencies (eigenvalues) which are independent of the three stiffness coefficients and again represent unconstrained rigid body motion. For $k_{xz} = 0$, of course the two remaining values are those of the decoupled equation sets for k_{xx} and k_{zz} in equations (12a, c). But for $k_{xz} \neq 0$, the equation sets are coupled and different natural frequency values with coupled mode vectors will satisfy the eigenvalue/eigenvector problem.

Using the above formulation, an iterative approach to the experimental identification problem is to assume that reasonably good estimates of k_{xx} and k_{zz} are already available. These may be based on prior experimental measurements with simplified preload conditions or on the theoretical model, itself, under complex preload conditions but which has only been experimentally validated under simple preload conditions. The approach is iterative in that these estimates for k_{xx} and k_{zz} may need to be refined based on the approach predictions. Estimates for k_{xx} and k_{zz} along with measured natural frequencies and mode shapes of the eigenvalue problem of equation (13) may be used to solve for k_{xz} directly as follows:

$$\det \left\{ [\mathrm{BB}] - (k_{xz})^2 \left[\begin{bmatrix} 1 & -L_1 & -1 & -L_2 \\ -1 & L_1 & 1 & L_2 \end{bmatrix} [\mathrm{AA}]^{-1} \begin{bmatrix} 1 & -\mathrm{L}_1 & -1 & \mathrm{L}_2 \\ -1 & \mathrm{L}_1 & 1 & \mathrm{L}_2 \end{bmatrix}^{\mathrm{T}} \right] \right\} = 0, \quad (14)$$

where [AA] and [BB] are the left-hand arguments of equations (12a) and (12c), respectively. However, unless k_{xz} is significantly larger in value than the diagonal stiffness terms k_{xx} and k_{zz}, numerical difficulties will be encountered, particularly due to the inverse of [AA]. But, if $k_{xz} > (k_{xx}k_{zz})^{1/2}$, then one of the non-zero eigenvalues of equation (13) will become negative, which physically is not possible if the equations represent a stable system. In fact, for the typical bearing, the theoretical formulation predicts that k_{xz} will be an order of magnitude less than the values k_{xx} and k_{zz}. As an alternative iterative approach, given estimated values of k_{xx} and k_{zz}, the effect of k_{xz} on the coupled nondegenerate mode shapes of equation (13) can be utilized to estimate its value based on comparison with

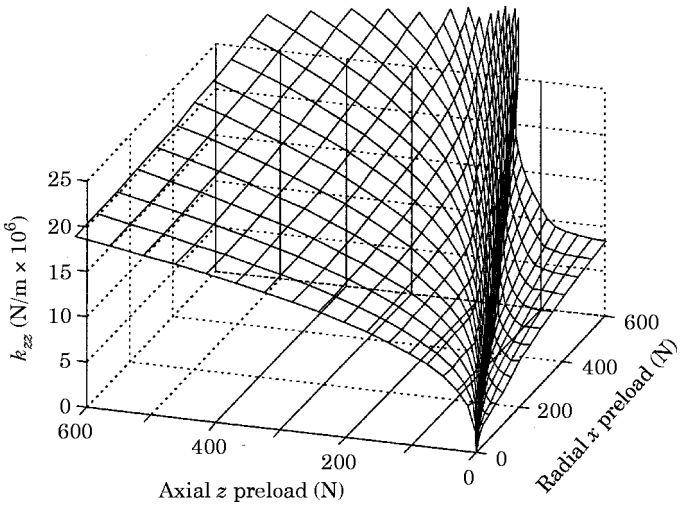

Figure 5. Linearized axial stiffness coefficient k_{zz} of bearing as a function of axial z and radial x preload conditions based on theory of section 4. Mesh displacement resolution: axial $2{\cdot}9 \times 10^{-6}$ m (0–$8{\cdot}41 \times 10^{-5}$ m shown), radial $5{\cdot}5 \times 10^{-7}$ m (0–$1{\cdot}595 \times 10^{-5}$ m shown).

experimental modal analysis of the test system. Details of an example case are given in section 6.

Calculation of k_{yz} in the presence of a y direction radial load *plus* an axial z direction load is identical to the procedure discussed above for k_{xz}. More generally, since the radial co-ordinate pair, x and y, can always be defined such that the resultant radial preload is oriented in the positive x direction, once values of k_{xx}, k_{yy}, k_{zz} and k_{xz} are obtained in this co-ordinate frame, a simple linear transformation can be used to obtain values for all six of the potentially non-zero stiffness and cross-coupling stiffness coefficients k_{xx}, k_{yy}, k_{zz}, k_{xz}, k_{xy} and k_{yz} for any other co-ordinate orientation.

6. EXAMPLE CASE RESULTS: EXPERIMENTAL VERIFICATION OF THEORY

An example study was undertaken using the system depicted in Figure 4. It was verified beforehand that the test masses are indeed rigid for the frequency range of interest. However, the rigidity of the bearing interface fixture relative to the bearing, particularly the inner stub, is an issue. The test setup is flexibly suspended and axial and/or radial preloads are applied across the bearing, again using flexible couplings with stiffness coefficients several orders of magnitude below those of the bearing. Note that the preloads must consist of equal forces of opposite direction applied along vectors which pass through the bearing pivot point to maintain static stability. An electrodynamic shaker with random excitation was used to excite the setup in the axial or radial direction. The frequency response is recorded and a polynomial curve fit of it is conducted in the vicinity of the resonance peak(s) to obtain the natural frequency(ies) and mode shape(s). Given system parameter values and ranges of axial (z) and radial (x and y) preload conditions, bearing stiffness coefficients are calculated based on the experimentally measured natural frequencies.

The self-aligning bearings which were tested were off-the-shelf items manufactured by SKF, Inc. Relevant dimensions of the bearing are provided in Table 1. Two rows of roller ball bearings are mounted on a fairly standard inner race and on an outer race with a center

TABLE 1

Parameter values for spherical bearing used in experimental study

$\alpha_0 = 12{\cdot}7$ deg.—undeformed contact angle	$d_0 = 42{\cdot}67$ mm—outer raceway diameter
$r_L = 0{\cdot}0015$ mm—radial clearance [Harris, 1984]	$r_i = 3{\cdot}75$ mm—inner raceway groove curvature radius
$z = 15$—number of balls per row	$\delta^* = 0{\cdot}6355$—dimensionless contact deformation [8]
$D = 7{\cdot}131$ mm—ball diameter	
$d_i = 27{\cdot}8$ mm—inner raceway diameter	

of curvature coincident with bearing geometric center. Hence, rotational orientation of the inner race with respect to the outer race is unrestrained about all three axes.

Theoretical calculations of the linearized bearing stiffness and cross-stiffness coefficients as a function of axial z and radial x preloads are shown in Figures 5–8. There are three direct stiffness and three-cross-coupling stiffness coefficients. Under simple radial or axial preloading conditions alone, all cross-stiffness coefficients are negligible. In other words, the matrix of equation (7) is diagonal. Under combined axial z and radial x preloading, the cross-stiffness coefficient k_{xz} becomes non-zero, as shown in Figure 8. The other two cross-stiffness coefficients, k_{xy} and k_{yz}, remain negligible and hence are not shown graphically. Mesh displacement resolution in the figure captions refers to the incremental bearing displacements, axial and radial, which were used to generate the three dimensional contour plot. In other words, from these plots, one can obtain the corresponding stiffness coefficient value as a function of radial and axial preloads as well as radial and axial bearing deformations. Mesh lines of constant axial displacement are roughly perpendicular to the direction of changing axial preload and mesh lines of constant radial displacement are roughly perpendicular to the direction of changing radial preload.

Experimental calculations of the linearized bearing stiffness coefficients under simple preload conditions (axial *or* radial) are shown in Figure 9. Theoretical stiffness coefficient values are estimated using the method described in section 5 under the assumption that cross-stiffness coefficient values are negligible. Experiment and theory compare favorably for axial stiffness, k_{zz}, predictions. However, radial stiffness k_{xx} predictions and experiment

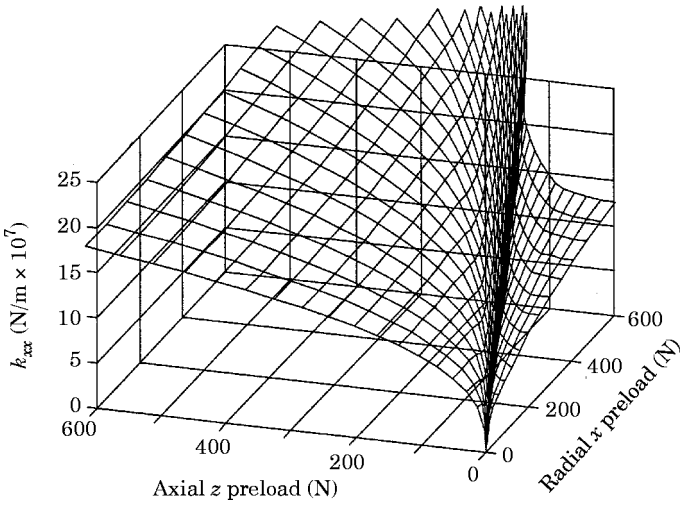

Figure 6. Linearized radial stiffness coefficient k_{xx} of bearing as a function of axial z and radial x preload conditions based on theory of section 4. Mesh displacement resolution: axial $2{\cdot}9 \times 10^{-6}$ m (0–$8{\cdot}41 \times 10^{-5}$ m shown), radial $5{\cdot}5 \times 10^{-7}$ m (0–$1{\cdot}595 \times 10^{-5}$ m shown).

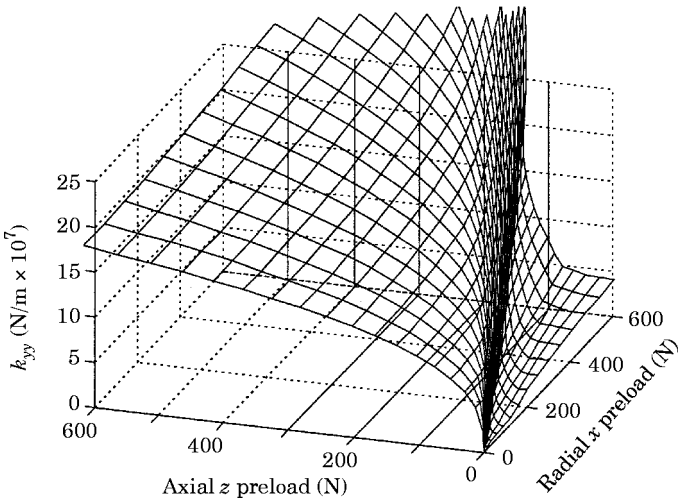

Figure 7. Linearized radial stiffness coefficient k_{yy} of bearing as a function of axial z and radial x preload conditions based on theory of section 4. Mesh displacement resolution: axial $2{\cdot}9 \times 10^{-6}$ m (0–$8{\cdot}41 \times 10^{-5}$ m shown), radial $5{\cdot}5 \times 10^{-7}$ m (0–$1{\cdot}595 \times 10^{-5}$ m shown).

show discrepancy. It is believed that at least some of this discrepancy is due to the compliance of the bearing fixture, particularly the inner stub. As a first approximation, the inner stub may be modelled as a uniformly loaded cantilever beam as shown in Figure 10. Based on static theory, its effective lateral stiffness, k_{st}, representing the ratio between the applied force and deflection at the midpoint which is aligned with the bearing center is given as [13]

$$k_{st} = (4/17)96EI/L^3, \tag{15}$$

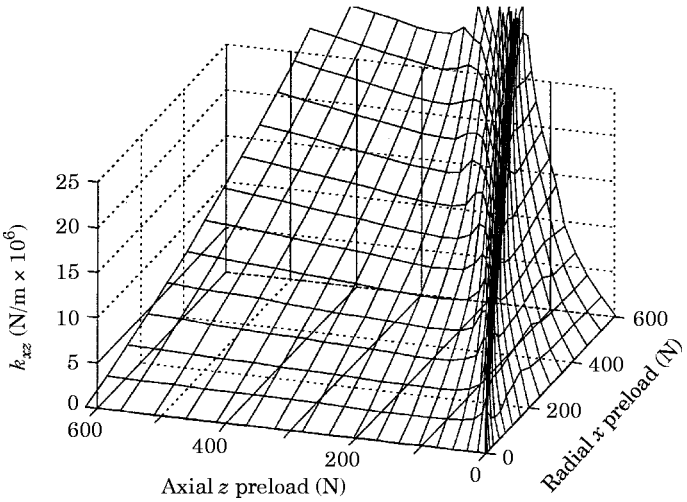

Figure 8. Linearized radial–axial cross-coupling stiffness coefficient k_{xz} of bearing as a function of axial z and radial x preload conditions based on theory of section 4. Mesh displacement resolution: axial $2{\cdot}9 \times 10^{-6}$ m (0–$8{\cdot}41 \times 10^{-5}$ m shown), radial $5{\cdot}5 \times 10^{-7}$ m (0–$1{\cdot}595 \times 10^{-5}$ m shown).

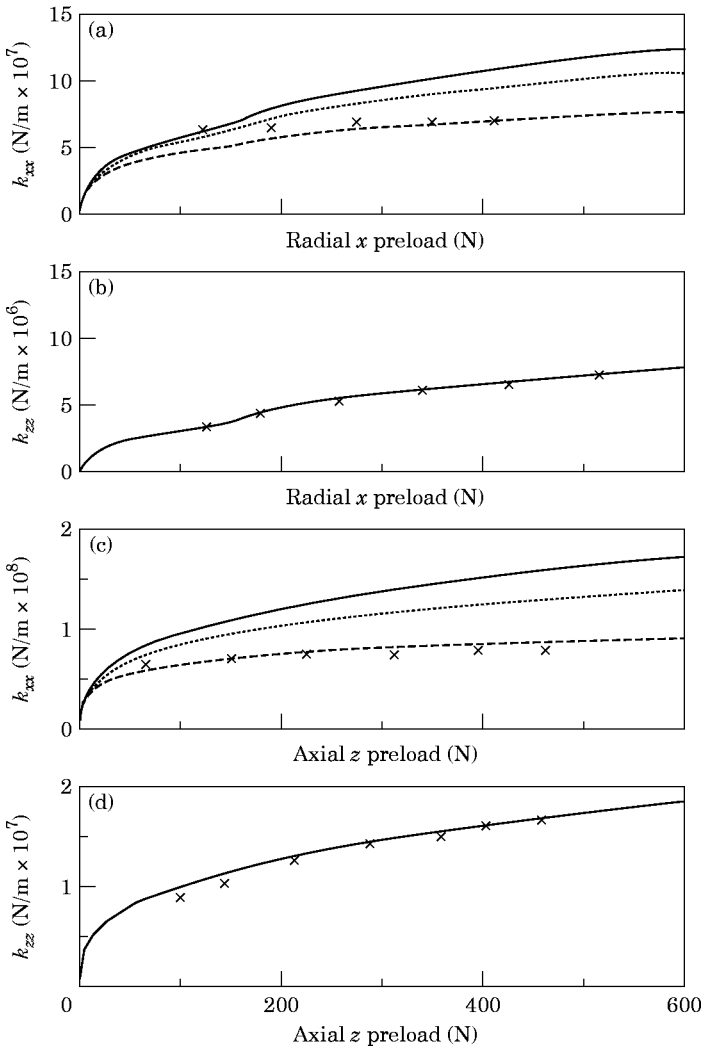

Figure 9. Linearized bearing stiffness coefficients. Comparison of theory and experiment for simple preload conditions. (a) Radial stiffness k_{xx}/radial preload x; (b) axial stiffness k_{zz}/radial preload x; (c) radial stiffness k_{xx}/axial preload z; (d) axial stiffness k_{zz}/axial preload z. Key: ——, theoretical calculations based on section 4 (·····, with theoretically calculated bearing fixture compliance; -----, with empirically added fixture compliance); × × × ×, experimental calculations based on section 5.

where variables are defined in Figure 10. For the experimental test rig, $k_{st} = 7{\cdot}5 \times 10^8$ N/m. If this is considered in series with the bearing radial stiffness term in the theoretical prediction of the net radial stiffness, theory follows experiment more closely as shown in

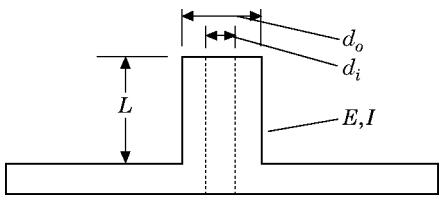

Figure 10. Cantilever stiffness approximation for inner stub of bearing fixture. Here $E = 1{\cdot}9 \times 10^{11}$ N/m^2 (stainless steel), $I = \pi/64(d_0^4 - d_i^4)$, $L = 0{\cdot}0257$ m, $d_0 = 0{\cdot}01585$ m, $d_i = 0{\cdot}0071$ m.

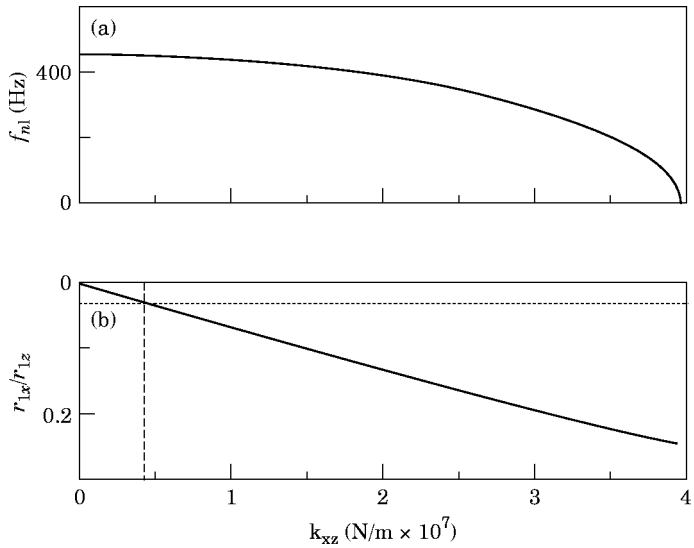

Figure 11. Experimental test setup parameter values as a function of cross-coupling stiffness coefficient k_{xz}. Axial preload = 200 N; radial preload = 160 N; $k_{xx} = 1{\cdot}23 \times 10^8$ N/m; $k_{zz} = 1{\cdot}27 \times 10^7$ N/m (based on theory of section 4). Key: (a) —, Lower non-degenerate natural frequency of test setup (equation (13)); (b) ———, associated mode shape ratio r_{1x}/r_{1z} (equation (13)); ·····, experimentally measured mode shape ratio; - - - -, theoretically predicted value for k_{xz}.

Figure 9. By empirically adding additional radial compliance in the bearing fixture ($k_{st} = 2 \times 10^8$ N/m), perhaps from the outer ring or the inner stub, theory and experiment can be brought to a closer match as shown in the figure.

Given estimates for the direct radial and axial stiffness coefficients, the cross-stiffness coefficient, k_{xz}, can be estimated under the combined radial plus axial preload condition as proposed in section 5 by comparing theoretical and experimental calculations of the coupled mode shapes. In Figure 11(a), the first non-zero natural frequency of the

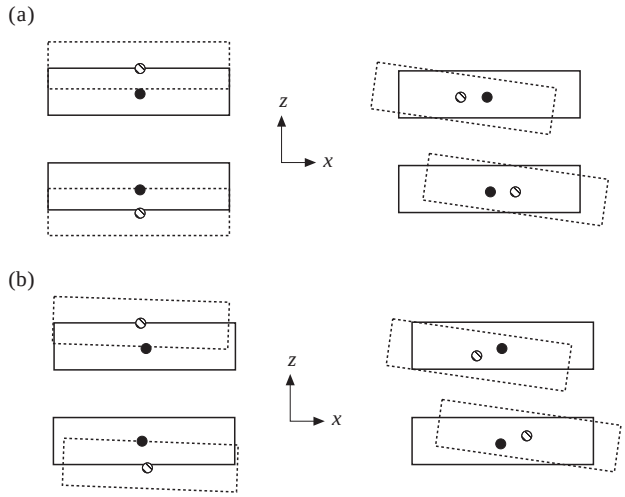

Figure 12. Typical test fixture mode shapes and natural frequencies for different preload conditions. (a) Simple preloading (axial *or* radial); (b) composite preloading (axial *plus* radial). Key: —, undeformed shape (●, center of gravity); - - - -, deformed shape (○, center of gravity). Left column $f_{n1} = \sigma$ (450 Hz); right column $f_{n2} = \sigma$ (1300 Hz).

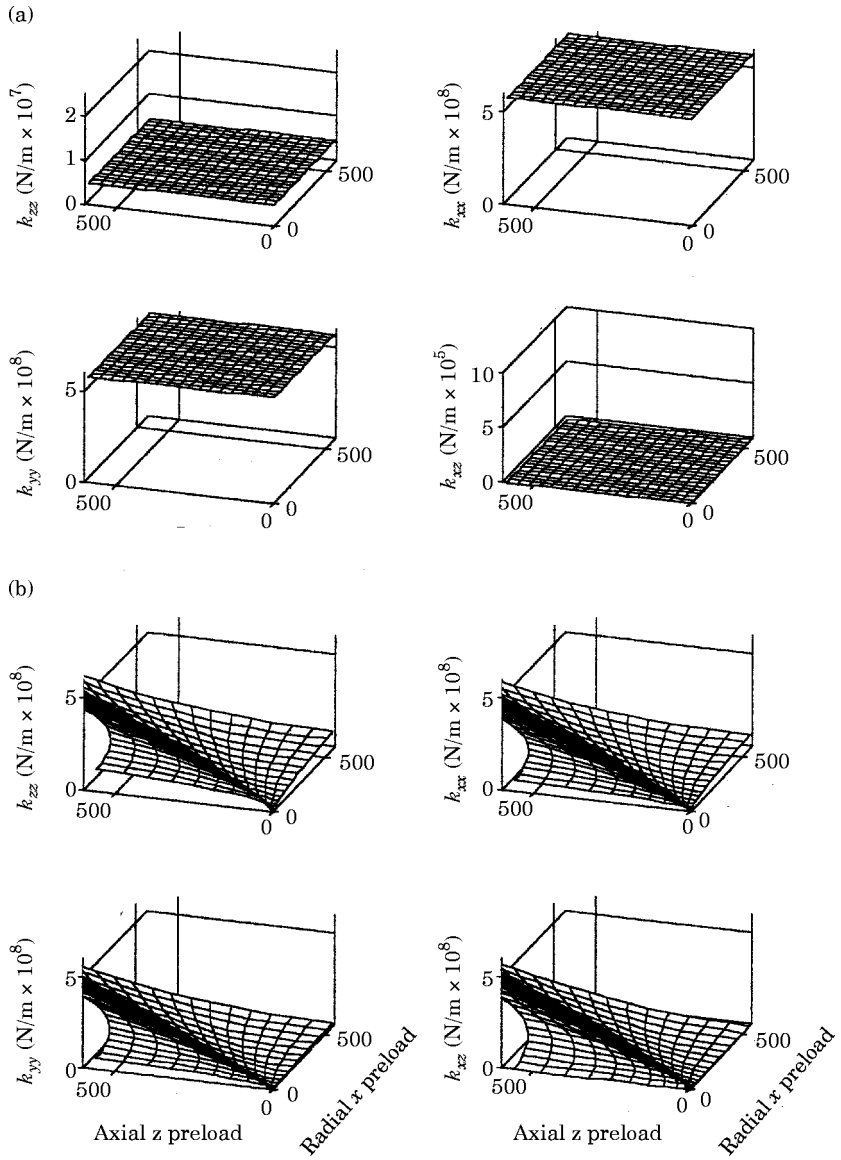

Figure 13. Stiffness coefficients for different unloaded contact angles, α_0. (a) $\alpha_0 = 0°$, mesh displacement resolution: axial 7×10^{-6} m (0–$1{\cdot}19 \times 10^{-4}$ m shown), radial 5×10^{-8} m (0–1×10^{-6} m shown). (b) $\alpha_0 = 45°$, mesh displacement resolution: axial 7×10^{-7} m (0–$1{\cdot}68 \times 10^{-5}$ m shown), radial 9×10^{-7} m (0–$2{\cdot}34 \times 10^{-5}$ m shown).

experimental test system is shown as a function of k_{xz} given values of k_{xx} and k_{zz} which are based on the theoretical model for the given axial *plus* radial preload condition. Note that the change in natural frequency as a function of k_{xz} is non-linear with a very minimal slope at the lower stiffness values and a value approaching zero as k_{xz} approaches $(k_{xx}k_{zz})^{1/2} = 3{\cdot}95 \times 10^7$ N/m. In Figure 11(b), the ratio of the radial motion r_{1x} over the axial motion r_{1z} of the center of gravity of the first rigid body in the test setup is shown as a function of k_{xz}. Note that this ratio is a linear function of k_{xz} and hence, provides more uniform and better resolution at lower k_{xz} stiffness values. Also plotted in Figure 11(b) is the experimentally measured mode shape ratio of r_{1x} to r_{1z} and the theoretically predicted

value of k_{xz} for the particular axial *plus* radial preload condition. The experimental mode shape ratio and the theoretical value for k_{xz} both intersect the r_{1x}/r_{1z} versus k_{xz} curve at nearly the same location. Hence the theoretical estimate of k_{xz} for this preload condition is reasonably accurate since using it results in a theoretical mode shape ratio r_{1x}/r_{1z} that is very similar to the experimentally measured ratio. This same comparison of theory and experiment was carried out for several other complex preload conditions with similar favorable results. In Figure 12, the non-degenerate mode shapes for the simple and composite preload conditions are shown. For the simple preload conditions, axial and radial motion of the centers of gravity of the test setup masses are decoupled. For the

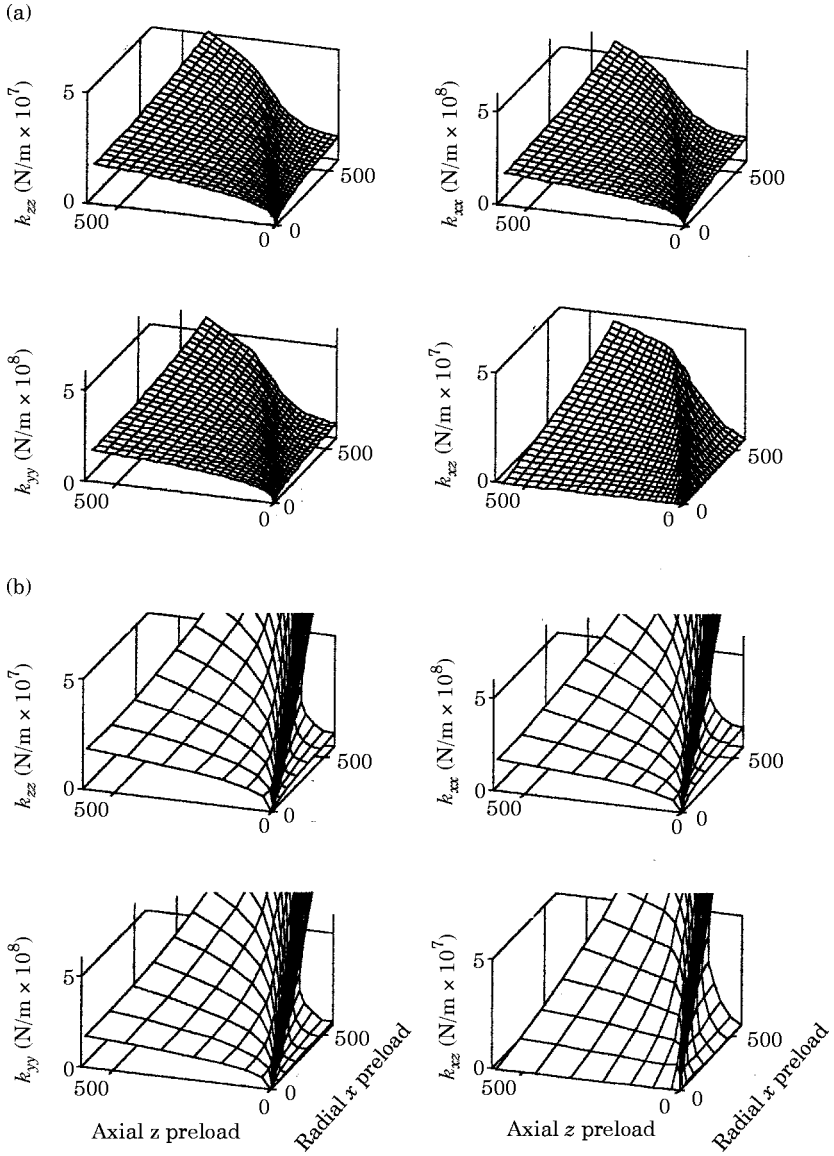

Figure 14. Stiffness coefficients for different radial clearances, r_L. (a) $r_L = 0$ mm, mesh displacement resolution: axial 2×10^{-6} m (0–$4{\cdot}8 \times 10^{-5}$ m shown), radial $2{\cdot}5 \times 10^{-7}$ m (0–7×10^{-6} m shown). (b) $r_L = 0{\cdot}005$ mm, mesh displacement resolution: axial 7×10^{-6} m (0–$1{\cdot}61 \times 10^{-4}$ m shown), radial $1{\cdot}3 \times 10^{-6}$ m (0–$3{\cdot}51 \times 10^{-5}$ m shown).

composite preload condition, coupling occurs. Additionally, this degree of coupling is dependent on the composite preload level. In terms of a typical shaft–bearing–plate system, such as shown in Figure 1, this coupling condition implies that transverse excitation of the shaft in the x direction will result in out-of-plane transverse vibration of the flexible casing in the z direction.

7. PARAMETRIC STUDIES

The nature of the spherical bearing stiffness matrix as a function of system parameters is briefly investigated further by varying the unloaded contact angle, α_0, and the radial clearance, r_L. The stiffness coefficients for two different contact angles, one greater than and one less than that of the base case (Figures 5–8), are shown in Figure 13. Note that for $\alpha_0 = 0$, the variation in stiffness coefficient values is much less over the shown range of preload levels. Hence, the applicability of a linear stiffness matrix to represent the bearing may be valid over a wider dynamic force operating range. The stiffness coefficients for two different radial clearance levels, one greater than and one less than that of the base case (Figures 5–8), are shown in Figure 14. Here, as in Figures 5–8 and 13, bearing relative displacement is depicted by the mesh resolution in the three-dimensional contour plot. The mesh resolution value is given in the figure caption. If one takes into account the differences in mesh resolution between Figures 14(a) and 14(b), it is seen that the radial clearance has a relatively minimal effect on the shape of the stiffness coefficient contours but a significant effect on the resulting relative displacement across the bearing with respect to a given preload.

8. CONCLUSION

A new theoretical model for the direct and cross-coupling stiffness coefficients of self-aligning (spherical) rolling element bearings has been developed and partially validated using new experimental techniques. The validation is partial in that only a finite number of preload conditions, both simple and complex, have been considered. Additionally, there is ambiguity in some of the experimental results due to unquantified dynamics in the test fixture. Nonetheless, the theoretical and experimental results show that stiffness coefficient values are complex functions of radial and axial preloads. While cross-coupling stiffness coefficients are negligible with simple radial or axial preloads, under the combined radial plus axial preload condition, the cross-coupling stiffness coefficient between the axial direction and the direction of the radial preload becomes significant. This cross-coupling parameter may play a significant role in the transmission of vibratory energy in the typical shaft–bearing–plate application coupling transverse shaft vibrations to transverse plate vibrations. Armed with the spherical bearing model of this study and comparable models of other researchers for conventional moment carrying bearings, comparative studies of vibratory energy transmission in typical compliant shaft–bearing–plate systems using the alternative types of bearings are in progress and will be reported in a future article.

ACKNOWLEDGMENT

The support of the U.S. Department of Energy, Office of Basic Energy Sciences-Materials Sciences, under contract no. W-31-109-ENG-38, is acknowledged.

REFERENCES

1. A. D. Dimarogonas and S. A. Paipetis 1983 *Analytical Methods in Rotor Dynamics*. London: Applied Science.
2. J. S. Rao 1983 *Rotor Dynamics* New York: John Wiley.
3. I. Basdogan and T. J. Royston 1998 *Journal of Vibration and Control* (accepted). A theoretical and experimental study of the vibratory dynamics of high precision optical positioning systems.
4. T. C. Lim and R. Singh 1990 *Journal of Sound and Vibration* **139**, 179–199. Vibration transmission through rolling element bearings, part I: bearing stiffness formulation.
5. T. C. Lim and R. Singh 1990 *Journal of Sound and Vibration* **139**, 201–225. Vibration transmission through rolling element bearings, part II: system studies.
6. T. C. Lim and R. Singh 1994 *Journal of Sound and Vibration* **169**, 547–553. Vibration transmission through rolling element bearings, part V: effect of distributed contact load on roller bearing stiffness matrix.
7. R. J. Kleckner and J. Pirvics 1982 *Transactions of the American Society of Mechanical Engineering*, *Journal of Lubrication Technology* **104**, 99–108. Spherical roller bearing analysis.
8. T. A. Harris 1984 *Rolling Bearing Analysis*, *Second Edition*. New York: John Wiley.
9. A. B. Jones 1960 *Transactions of the American Society of Mechanical Engineering*, *Journal of Basic Engineering* **82**, 309–320. A general theory for elastically constrained ball and radial roller bearings under arbitrary load and speed conditions.
10. T. L. H. Walford and B. J. Stone 1980 *Institute of Mechanical Engineers*, *Journal of Mechanical Engineering Science* **22**, 175–181. The measurement of the radial stiffness of rolling element bearings under oscillating conditions.
11. J. Kraus, J. J. Blech and S. G. Braun 1987 *Transactions of the American Society of Mechanical Engineering*, *Journal of Vibration*, *Acoustics*, *Stress*, *and Reliability in Design* **109**, 235–240. *In situ* determination of rolling bearing stiffness and damping by modal analysis.
12. R. Tiwari and N. S. Vyas 1995 *Journal of Sound and Vibration* **187**, 229–239. Estimation of non-linear stiffness parameters of rolling element bearings from random response of rotor–bearing systems.
13. J. E. Shigley and C. R. Mischke 1989 *Mechanical Engineering Design*. New York: McGraw-Hill; fifth edition.